ISSN No:-2456-2165

Comparison between 3D Printed Auxetic and Non-Auxetic Structures: Simulation and Experimental Validation

Josewin Lawrensen [1,2], Aamer Nazir [1,2],* and Chi-Pin Hsu [1,2]
[1] High Speed 3D Printing Research Center, National Taiwan University of Science and Technology, No. 43, Section 4, Keelung Road, Taipei 106, Taiwan, R.O.C
[2] Department of Mechanical Engineering, National Taiwan University of Science and Technology, No. 43, Section 4, Keelung Road, Taipei 106, Taiwan, R.O.C

Abstract:- In this study, five different auxetic structures were designed into dog bone specimens and printed with approximated similar masses, intended as the constant parameter. These specimens were then simulated by Finite Element Analysis before being subjected to tensile testing. In the simulation, yield stress comparisons between auxetic structures and non-auxetic were analyzed. UTS (Ultimate Tensile Stress) and maximum strain from tensile test results were compared with 3D printed non-auxetic with concentric infill. The results showed agreement between simulation and testing in terms of deformations and failure spots. In the end, simulated auxetic structures showed extensions in yielding limit at a range of 5-20% compared to control. Meanwhile, four out of five tested auxetics were proved to gain increment in UTS value at a range of 25.14%-160.9% and additional maximum strain percentage by 4.1-31.49% compared to non-auxetic with 10.1 MPa and 2.48%, UTS and maximum strain Respectively.

Keywords:- *Additive Manufacturing; Auxetic Structure; Finite Element Analysis; Tensile Test; Polylactic Acid.*

I. INTRODUCTION

3D printing technology has revolutionized the manufacturing industry at an exponential rate by providing practical and reliable processes for manufacturing highly complex structures[1]. There are a lot of 3D printing methods such as stereolithography, selective laser sintering, fused deposition modeling, etc.[1]. Fused deposition modeling (FDM) is well known as the cheapest method in additive manufacturing[2]. Polylactic Acid (PLA), which makes plastic glasses and straws, is also widely applied in 3D printed parts due to its low cost. Derived from organic materials, PLA is environmentally friendly since it is recyclable[3]. Thus, we chose FDM and PLA as printing methods and materials respectively in this study.

The auxetic structure is the material structure that has a negative Poisson's ratio, which means it expands longitudinally with the direction of tensile force; on the other hand, it shrinks longitudinally with the direction of compression force. Research has been conducted to use the potential of this structure from energy absorption purposes [4], such as auxetic foam[5] to tunable microfilter[6]. Auxetic structures that are applied in 3D printed can be even more beneficial since we can improve the mechanical properties of the structure itself [7]. High energy absorption protective gears can be produced and applied in sport [4]. Military blast shock wave protection panel wear which significantly prevent and reduce chance of injuries even life losses [8]. The application of auxetic structure even expands to aerospace, biomedical, chemicals and sensor-actuators application due to enhanced shear modulus, indentation resistance and fracture toughness [9].

There are a lot types of auxetic structure and it is crucial to study the behavior and properties of each of them in order to determine the best structure for specific design purpose. Especially, their behaviors under loading situation. It is shown in clearly that different auxetic structures behave uniquely under impact loading[10].

Due to porous structure, auxetic structures might have lower value of stiffness. This negative drawback can be compensated by shrinking into molecular auxetic or auxetic nanomaterials in future research as it can increase modulus value[9]. For now, the manufacturing of tiny auxetic structures via 3D printing technologies is halted by parameters that disable the possibilities to go even micro-size level.

II. METHODOLOGY

A. Design

2D designs were generated using AUTOCAD 2020 since its faster performance and compatibility with average computer (,a). The dimensions used were not real dimensions. Thus, conversion to real dimensions was adopted (Table 1, Fig 2) through other software, Fusion 360 (Fig 1,b). By measuring the scale between these two software, we can determine the precise real dimensions of 2D sketches. Then, CAD files were converted into 3D models using Fusion and exported as STL file, which was a standard file for FDM 3D printers. Using SpaceClaim 2021, which was the design modeler for ANSYS Mechanical, STL models were verified for defects and finalized for simulation purposes (Fig 1,c). Finally, STL models were meshed and simulated by the Finite Element Analysis (FEA) method (Fig 1,d).

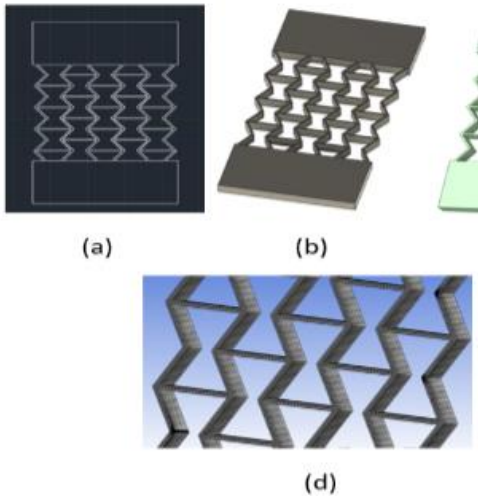

Fig. 1. Designing process (a) 2D modeling on Autocad 2020; (b) 3D modeling on Autodesk Fusion 2020: (c) importing the 3D model to design modeler; (d) Meshing of 3D model prior to FEA (Finite Element Analysis) on ANSYS.

The specimen width was 50 mm in terms of length that was available for designing auxetic specimens instead of the specimen's actual width, which varied uniformly depending on the geometry of each auxetic specimen.

Table 1. Dimension of Specimens

Width	25 mm
Specimen Length	58 mm
Grip Length	25 mm
Thickness	6 mm
Grip Cross Section Area	$3x10^{-4}$ mm^2

Fig. 2. Dimensions of Model

The models were designed in iterative trial and error way to make sure the masses were similar to each other. Beside, their thicknesses and lengths were also designed to be exact. The purpose of these constraints were to make sure that structural design was chosen as independent variable in this study. At the end, five auxetics, a non auxetic (Control) and an ANSYS topology optimized model were proposed (Fig 4, a-g). Purpose of optimization on models was to generate the most efficient design with minimized mass as main purpose. This is very crucial to solve many problems in manufacturing area. For example, material saving structures that is strong enough for specific requirement safety factor. Topology results are mostly crude and hard to be manufactured. Thus, final and further editing on model is a must. ANSYS Mechanical provided varying and helpful tools on optimization models. First, exclusion regions were selected (both grips) (Fig 3,a). Then, response constraint was determined to be 50 %, in other words, the maximum allowed mass reduction was 50 %. Finally, the computational results were given through 500 iterations (Fig 3,b). The schematic for optimization process were shown (Fig. 3,c).

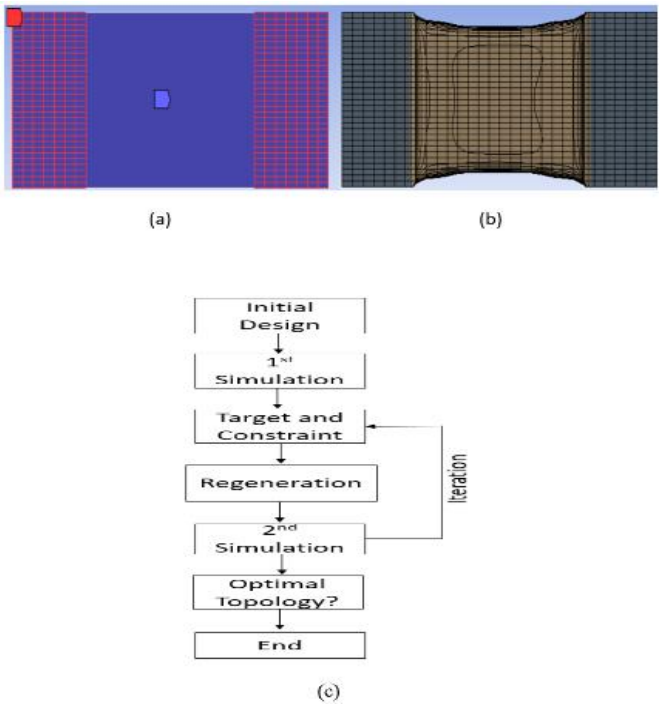

Fig. 3. Optimization Control Process (a) exclusion region shown in red; (b) Optimized Version of Control; (c) Process Schematic

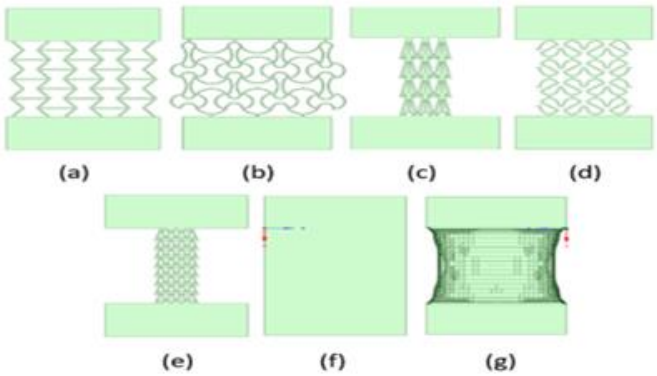

Fig. 4. (a) Model 1; (b) Model 2; (c) Model 3; (d) Model 4; (e) Model 5; (f) Control; (g) Optimized Control

B. Simulation Framework

In this study, ANSYS Mechanical Workbench was used as simulation software. However, it was considered as the most powerful software for FEA, some problems were encountered due to student version limitation and lack of computational power. Fortunately, all models were successfully simulated at the end. The purpose of this simulation was to determine the force required for each model to experience failures or to reach yield stress by applying varying tensile loadings.

Research had to be done as ANSYS Mechanical's material libraries did not provide any PLA properties, especially for 3D printed parts. Studies had been conducted to determine the properties of 3D printed PLA parts and

came out with some research papers. Since all of the specimens have thin-walled structures, the infill pattern generated by G-code was concentric. Thus, the properties of 3D printed PLA for concentric infill pattern were accumulated (Table 2); tangent modulus of elasticity, ultimate tensile stress, and young's modulus was taken from concentric infill pattern for ASTM D638-14 a standard piece[12]. Meanwhile, Poisson's ratio value was evaluated from the study on 3D printed rock mechanics[13]. Since Suitable yield stress input was not available, the approximation of its value was 3.9 MPa. Bulk modulus and shear modulus were automatically derived by ANSYS based on other properties' value.

Table 2. Properties Input for ANSYS Simulation

Properties	Value
Density	1250 kg/m^3
Young's Modulus	7.34 GPa
Poisson's Ratio	0.203
Bulk Modulus	4.119 GPa
Shear Modulus	3.0507 GPa
Yield Strength	3.90 MPa
Tangent Modulus	0.263 GPa
Tensile Strength	10.1 MPa

Since density value was obtained, with constant size of grips, mass without grips values were calculated (Table 3). For the same thickness (t=6mm), it was almost impossible to design models with the exact value of mass since each auxetic model had varying widths and structural densities.

Table 3. Mass of Each specimen

Model	Mass Without Grips
1	3.465 gr
2	3.520 gr
3	3.762 gr
4	2.920 gr
5	3.289 gr
Control	21.750 gr
Optimized Control	10.978 gr

The greatest challenge came from the meshing process since the right parameters such as; method, sizing, growth rate, etc. must be determined properly. Different types of geometries required specific parameters to be successfully meshed. Hex dominant method generated cubic meshes which was mostly desired for every model (Fig 1,d). Unfortunately, it costed a lot of time and computational power, which was way larger compared to other methods such as tetrahedrons (Fig 6,b). Alternatively, the sweep method was implemented to get cubic meshes even though the results were not as good as hex dominant's. Sizing and growth rate were also important factors as finer meshes provided detailed and accurate results. In this study, edge sizing with varying numbers of divisions and hard bias mode were used. It was important to make sure that the number of meshes did not exceed ANSYS Student Version limitation.

In tensile test simulation, one of the grip was constrained as fixed support meanwhile, the other grip was subjected to tensile force. To determine the failure force, another trial and error method was adopted. It took some time to guess the failure propagation force around the yield stress point. As increased force only resulted in constant stress value around yield point. Red cross section showed given force area (Fig 5,a). Blue cross sections were constrained (Fig 5,b)

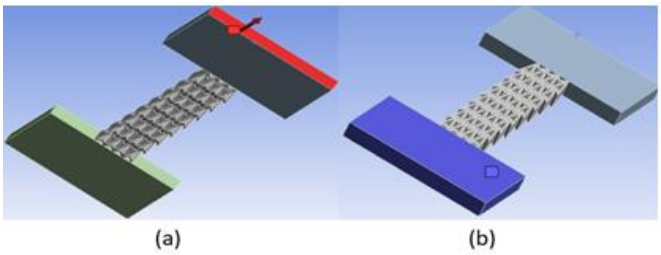

Fig. 5. Topology Optimization(a) force direction and selection; (b) Fixed Support Selection.

From the simulation results, how each model deformed before it failed was observed (Fig 6,a-g). Auxetic behaviors of each specimen were shown clearly that structures expanded longitudinally perpendicular with the direction of force instead of shrinking. On the other hand, control and its optimized version behave statically without any significant deformations. Auxetic structures were reported for their flexibility and large elastic deformations behavior[14]. Thus, these properties were beneficially applied in piezoelectric sensors and actuators, which converted mechanical load into electrical pulse as sensitivity value increased[15]. 3D printed soft composites of these structures were applied as multiphase tunable acoustic filters by exploiting NPR (Negative Poisson's Ratio) behavior [16].

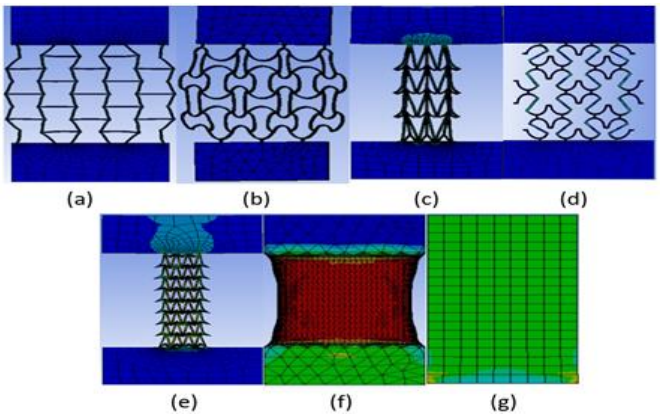

Fig. 6. ANSYS tensile simulation results (a) Model 1; (b) Model 2; (c) Model 3; (d) Model 4; (e)Model 5; (f) Control; (g) Optimized Control

All the results including topology optimized version were compared to control. It was interesting that yielding loads were varying even though the dimension of each models were constrained and the masses were similar to each other. Meanwhile, material saved of each specimen were also compared to control (Table 4). Load at yield for control and

optimized were much larger proportional to wider surface area comparing to auxetics.

Table 4. Simulation Yields and Material Saved Data

Model	Load at Yield	Material Saved
1	27 N	84.07%
2	37 N	83.82%
3	102 N	82.70 %
4	26 N	86.57%
5	175	84.87%
Control	2934 N	-
Optimized Control	2478 N	49.52%

By setting the simulation output as equivalent total strain and equivalent (Von Mises) stress relative to time, shear stress diagram of each models were plotted easily using chart function. Minimum and average values were eliminated since our interests on maximum value. Auto stepping mode was adjusted to have minimum value of 10 which meant at least the diagram would have 10 points. The results were not accurate enough, limitation on computation had limited the progress. Then, the data from 7 different models were transferred into MATLAB R2021a to construct clearer plots. At the end, comparison between shear stress diagram of each models were shown (Fig 7)

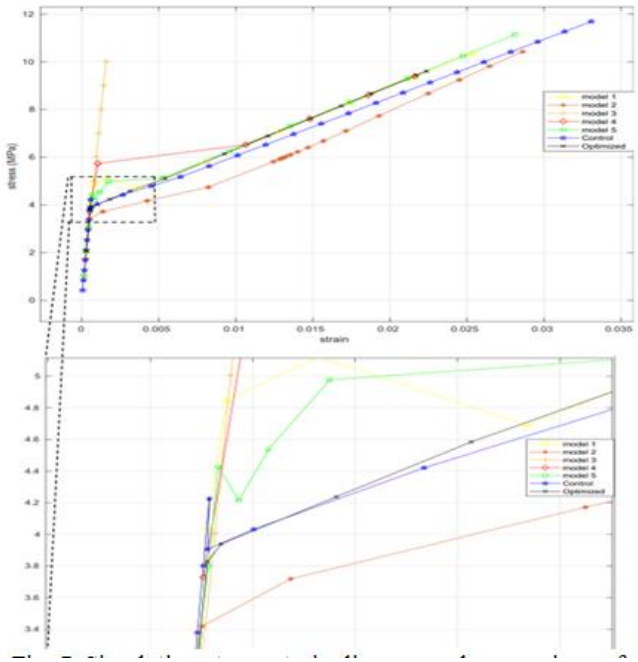

Fig. 7. Simulation stress-strain diagram and comparison of yields

Based on the stress-strain diagram analysis, the structural yielding stress values of each specimen were determined through an examination on the points at which the straight elastic regions ended (Fig 7). It showed that Model 3 had the highest yield stress (approx. 5.05 MPa) followed by Model 1 (4.84 MPa), Model 5 (4.42 MPa), Control (4.23 MPa), Optimized Control (3.82 MPa), Model 4 (3.73 MPa) and Model 2 (3.43 MPa). In conclusion, auxetic effects indeed pushed the elastic performance of non-auxetic by 5-20% based on simulation results.

C. Experimental Framework

In this study, only models 1-5 were printed for real testing. The parts were printed using an FDM 3D printer, Prusa i3 MK3S, Marlin as firmware, and PrusaSlicer as slicer program (Fig 8). Printing was set to be 100 % infill, 0.15 nozzle size with generic PLA as the material to make sure the printed properties were similar to the research paper mentioned[12]. Three parts were printed at the same time, five sets of the printing process each consumed approximately seven hours of printing time. In a total of fifteen models were printed at the end, three per each auxetic structure (Fig 9,a-e). Brim was also adjusted into the slicing process in to increase printing adhesive area.

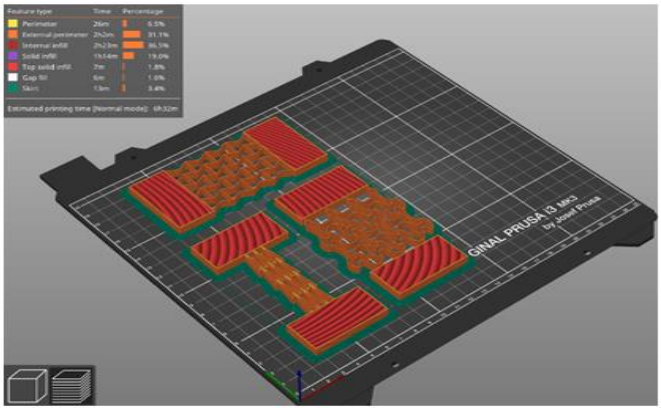

Fig. 8. Sliced Models in PrusaSlicer

Several specimens had warping defects and stringing problems even though they were not significant due to the nature of small size, complex design, and limitation on the printer. Overall, the results were totally fine, and this showed the FDM 3D printer's capabilities to print thin-walled structures. The grips were printed with grid pattern and concentric for the auxetic part, which was weaker[17]. If the wider auxetic structure was designed, the g-code would be able to generate the same grid infill pattern as the grips (Fig 9,f)

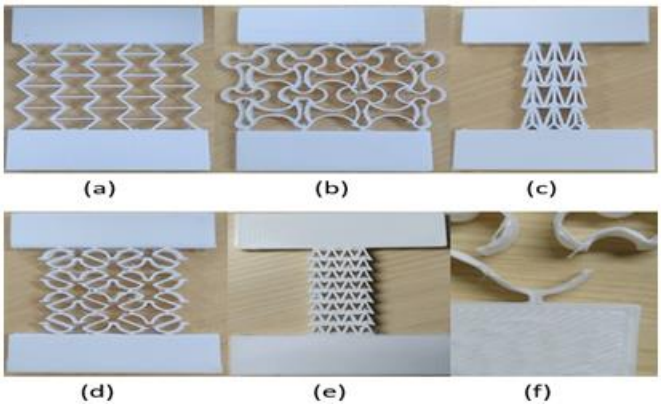

Fig. 9. Printed Models (a)Model 1; (b)Model 2; (c)Model 3; (d)Model 4; (f)Model 5; (g) Difference infill pattern between specimen and grip.

All of the specimens were labeled and measured to determine each of their thicknesses, widths, and lengths. These measurements were used as inputs for software applied in tensile testing. The measurements included an average of three different points for each parameter (Table 5). In order to deal with the varying non-uniform width values along with the specimens, the point with minimum structural width was observed, and the summation of actual minimum width was measured with a caliper. For example, in model 4, the summation of these four specimen-grip connectors widths (Fig 10) were chosen as the actual minimum width of the structure.

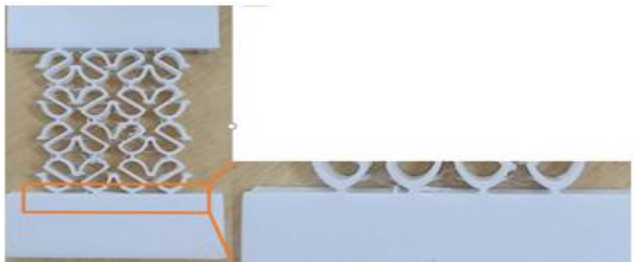

Fig. 10.Measurement Actual width of model 4

Table 5. Average Measurements Data of Each Specimens Printed (mm)

	Model 1			**Model 2**		
Specimen	**1**	**2**	**3**	**1**	**2**	**3**
Length	58.67	58.88	58.76	58.90	58.87	58.85
Min Width	5.23	5.21	5.45	3.45	3.67	3.66
Thickness	6.03	6.12	6.09	6.07	6.07	6.08
	Model 3			**Model 4**		
Specimen	1	2	3	1	2	3
Length	58.88	58.93	58.95	58.55	58.44	58.30
Width	7.78	7.86	7.89	6.55	6.78	6.89
Thickness	6.10	6.11	6.08	6.04	5.98	6.02
	Model 5					
Specimen	1	2	3			
Length	58.67	58.77	58.87			
Width	5.38	5.39	5.38			
Thickness	5.89	6.01	6.05			

All the specimens were tested using MTS Insight Electromechanical tensile tester machine (Fig 11) with the capacity of 10 kN. Testworks version 4 was compatible with the testing machine, which was trusted in this experiment. The three parameters that were measured before then were used as inputs for the software. Unfortunately, the width limitation input was 5.080 mm, and some of the specimen's widths exceeded the limit. Thus, further calculations were necessary to compensate for the errors. Besides the parameters, the pulling speed was adjusted to be 5mm/min.

The results showed the auxetic behaviors for each model as each of them expanded longitudinally perpendicular to the direction of tensile load except for model 3 (Fig 12,c), which did not show any significant behavior prior to failing. Results in model 1 (Fig 12,a) showed similar strain deformation of 3D printed piezoresistive auxetic strain sensor die[18] also stretchable and compressible auxetic foam piezoresistive sensor[19] due to improvement in sensor performance[20]–[22].

Fig. 11. Specimen and tensile testing module

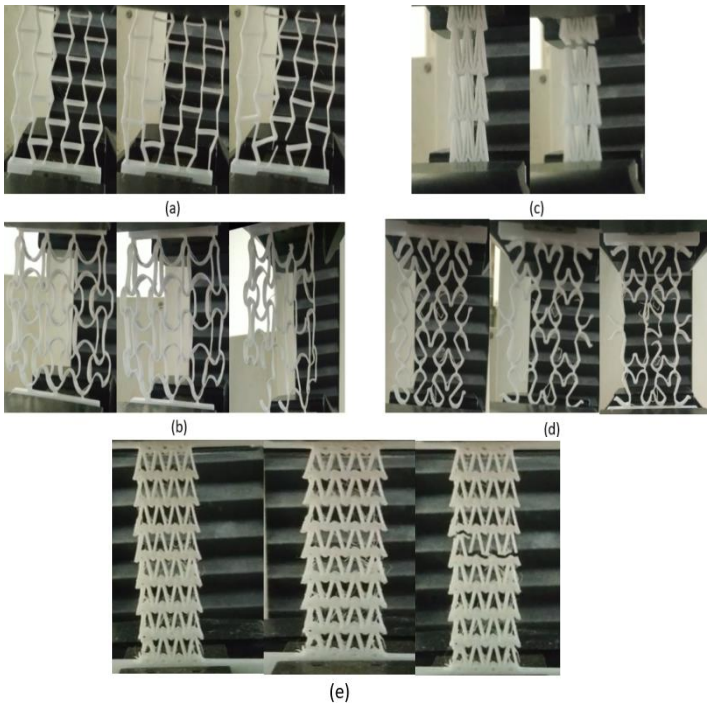

Fig. 12. (left to right) Before, during and after tensile test (a)Model 1; (b)Model 2; (c)Model 3; (d)Model 4; (e)Model 5

III. RESULTS

Comparisons between ANSYS and tensile testing results were conducted to determine the accuracy of ANSYS finite element analysis (Fig 13,a-e). The specimens in the simulation were subjected to load where the whole structure experienced previous input UTS value[12]. The red tags (Fig 13,a-e) showed the element where maximum stress happened at a given load. Thus, these spots were assumed to be the location in which breaking propagated in the real tensile test. The assumption agreed with the experimental results of all models. In model 2 (Fig 13,b) even predicted the plastic deformation of the whole structure that was tilted to the right side. ANSYS Finite Element Analysis results were also reasonably applied for design consideration. As shown in

model 3 (Fig 13,c), a huge concentration of stress located at the joint between specimen and grip caused it to fail instead of specimen parts. This means model 3 required modification for the sake of structural strength accuracy. The specimens were subjected to static structural instead of explicit dynamics analysis due to the limitation of computational power in which also limited post-failure deformation results. Thus, the stress strain curve post yielding stress was not accurate, and the point when each specimen actually broke was also unable to be processed. Overall, the ANSYS Finite Element Analysis has helped this study to illustrate and predict the deformation of each models, particularly, inside the elastic region. Noted that stress-strain curves values were not comparable between testing and simulation. The main reason was the inaccuracy of properties input on simulation.

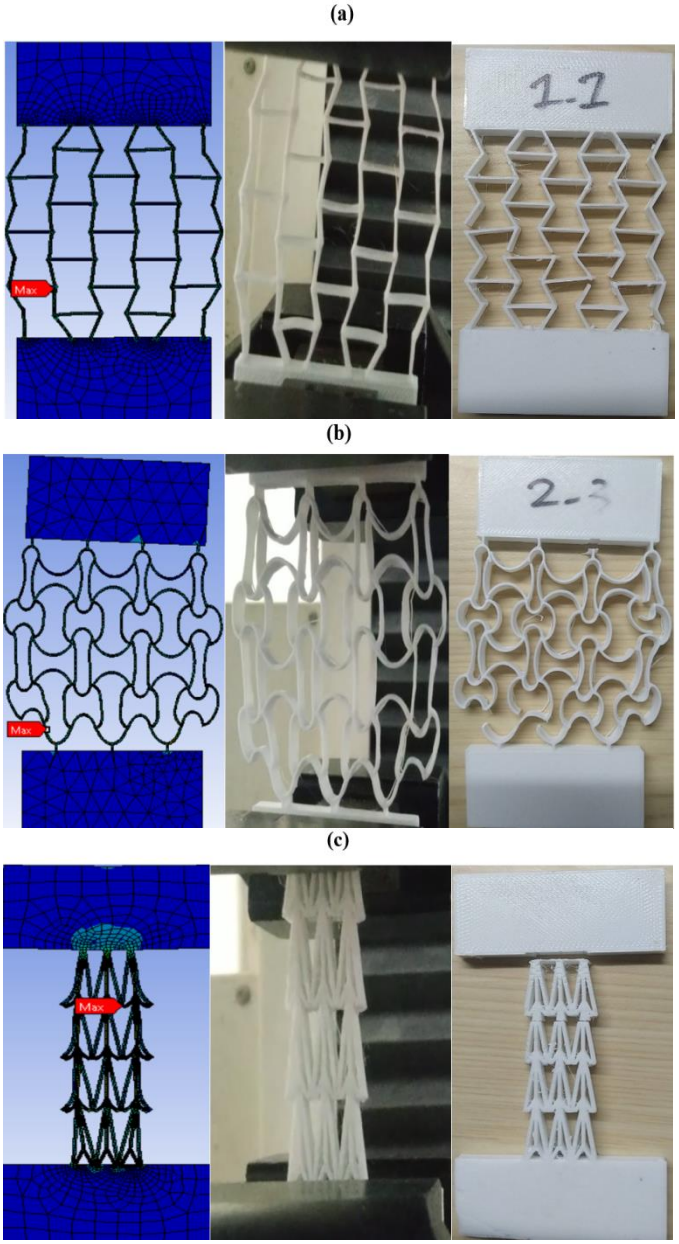

Fig. 13.Deformation comparison between simulation (left), testing (middle) and post failure (right) (a)Model 1; (b)Model 2; (c)Model 3; (d)Model 4; (e)Model 5

The data obtained from Testworks 4 were plotted, and the results were shown in the graphs for comparison. The diagonal axis showed strain percentage (%), vertical axis showed stress (MPa). Based on the curves, the behavior of each structure was explained. Model 3 (Fig 14,c) had the most brittle property compared to the other four specimens, followed by model 5 (Fig 14,e) had the tendency to be ductile. Model 1 (Fig 14,a) and 2 (Fig 14,b) showed similar ductile structure. Lastly, model 4 (Fig 14,d) acted plastic as it achieved maximum strain up to 33.97 %. By examining the elastic area, the yield stress values of each specimen were approximated (Fig 15).

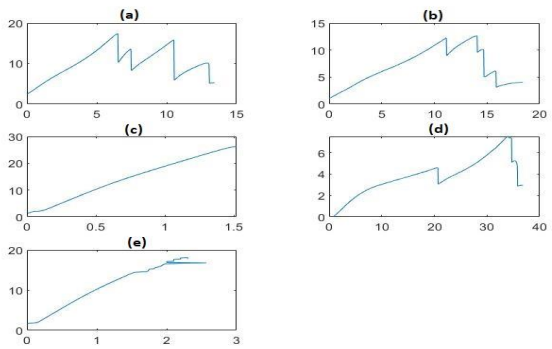

Fig. 14.Actual stress strain diagram of each model, horizontal axis represents strain percentage meanwhile vertical axis represents stress (MPa) (a)Model 1; (b)Model 2; (c)Model 3; (d)Model 4; (e)Model 5

Table 6. Experimental Data from Tensile Testing Compared with Non Auxetic (UTS= 10.1MPa, Max Strain Percentage=2.48%)

Model	Ultimate Tensile Stress (MPa)	Yield Stress (MPa)	Maximum Strain (%)	Increased UTS percentage	Additional Max Strain Percentage
1	17.37	7.5	6.58	71.98%	4.1%
2	12.64	5.4	13.97	25.14%	11.49%
3	26.35	27.5	1.52	160.9%	Decreased
4	7.514	4.7	33.97	Decreased	31.49%
5	18.14	13.9	2.30	79.6%	Decreased

From the data, model 3 had highest yield stress followed by model 5,1,2 and lastly 4 (Table 6). The order showed agreement with simulation yield orders even though some were reversed. The main reason behind errors in value was the properties input (Table 2) on ANSYS was based on paper references that used dog bone specimens as experimental parameters, which was different from the one that was implemented in this study. Another possibility was the simulated version of models was not considered as a layered structure with concentric infill. Even throughout this research time, many papers have published different values for 3D printed PLA properties value that was based on different dog bone options.

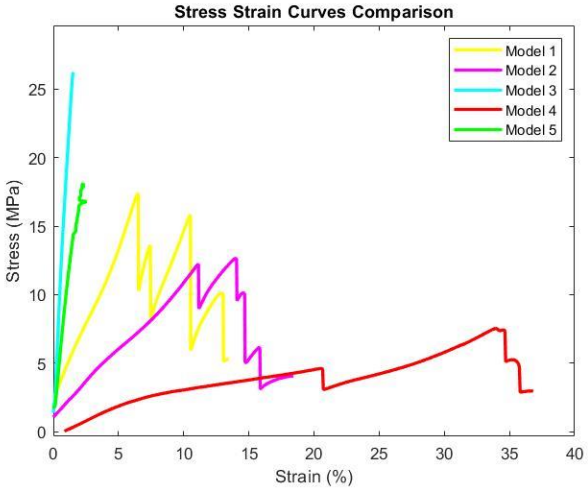

Fig. 15.Actual stress-strain diagram comparison of each specimen

Since the pieces were tested with the specification of ASTM D638-14, a dog bone design (Fig 16)(UTS=10.1MPa, Max Strain= 2.4%)[12] which has 41.6mm^2 minimum cross-sectional area subjected to load, a conversion should be made for each specimen that differed in cross-section area in order to get comparable results. The minimum total width and thickness were measured before; thus the ratio between average minimum area for each piece to dog bone was concluded for UTS revision (Table 7). In conclusion, auxetic structures had UTS value increased in the range of 25.14-160.9% and gave additional maximum strain percentage by 4.1-31.49% (Table 6) compared to non-auxetic concentric infill[12] except model 4 even without any converted revision due to smaller cross-section area.

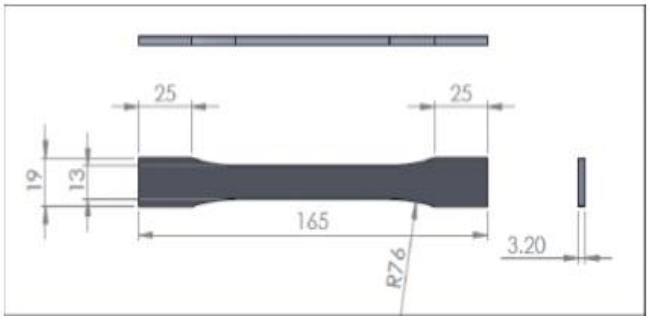

Fig. 16.ASTM D638-14 Dimension

Table 7. Ratio Comparison Between ASTM D638-14 and Specimens.

Model	Minimum Area (mm^2)	Ratio	UTS (MPa)	Revised UTS (MPa)
1	32.2	1.292	17.37	22.44
2	21.82	1.906	12.64	24.09
3	47.81	0.87	26.35	22.9245
4	40.529	1.0264	7.514	7.712
5	32.21	1.292	18.14	23.43

IV. DISCUSSIONS

The purpose of this study was to analyze the effects of implementing various auxetic shapes' behaviors and compare them with non-auxetic structures. Five different auxetic models with similar masses were simulated prior to printing and testing. Both results retrieved from FEA simulation and tensile testing showed improved mechanical properties, including; yield stress, UTS, and maximum strain compared to non-auxetics even with the reduction in material usage. Noted several important points retrieved from this experiment :

1.The designs used in the experiment had different parameters used and admitted widely. Difficulties in designing an auxetic structure with varying uniform widths into standard parameter dog bone structure (Fig 16) had halted the accuracy of these experiments. In the future, a standard for auxetic structure testing should be declared for tensile testing.

2.ANSYS FEA Simulation successfully predicted the failure and deformations of each structure. Failure spots were accurately predicted (Fig 13, a,-e) since the results were fully based on the geometry instead of the properties of the structure. Once the models are well-meshed, any deformations and failure of each element under yield stress (elastic region) can easily be determined using static

structural analysis. On the other hand, the stress-strain diagram was accurate enough to determine the order of yield strength even some errors occurred. Since it was limited to simulate the layered structure of 3D printed parts. In addition, the standard material properties for 3D printed PLA was widely varying from one paper to others[12], [13], [17] even with similar parameters; infill pattern and density. ANSYS required properties' input prior to simulation, but it did not provide any of them. In the future, ANSYS should give the corrected standard for 3D printed PLA.

3.Since the detection of failure spots was accurate for all five models (Fig 13,a-e), ANSYS FEA was granted trust to determine whether model modifications were necessary. As seen in model 3 (Fig 13,c), stress concentrated on joints seemed responsible for failure more than maximum stress occurred.

4.Static structural analysis only worked accurately at and below the yielding point, as it was unable to simulate plastic deformation/ breaking of materials. In the future, with greater computational power, rigid dynamics analysis can be performed to get the solutions. In other words, plastic deformation post-yielding can be simulated. Thus, a better and accurate stress-strain comparison able to be generated.

5.After comparing tensile tested models with concentric infill pattern testing[12]. Auxetic structure tremendously increased the UTS by 25.14-160.9 % and gave additional maximum strain percentage by 4.1-31.49% (Table 6) even though some of the structures had the minimum cross-section area less than ASTM D638-14 standard (Fig 16). The same results showed on ANSYS, as the auxetic UTS increased by 5-20% compared to the control value (Fig 7,b). Further experiments need to be conducted to verify this value.

6.In the future, thin-walled structures should be avoided to open the chance of grid infill pattern to be generated and observed to see which one has better performance of 3D printed auxetic structures (Fig 10,a).

In the future, studies on 3D printed auxetic structures will be encouraged and suggested as it will open the full potential of these high strength-to-weight ratio materials, which is tremendously beneficial in many engineering fields. Compression testing on 3D printed auxetics is also recommended for future researches.

ACKNOWLEDGMENT

This work was fully supported by High-Speed 3D Printing Research Center, National Taiwan University Science and Technology (NTUST), Taiwan.

REFERENCES

[1]. T. D. Ngo, A. Kashani, G. Imbalzano, K. T. Q. Nguyen, and D. Hui, "Additive manufacturing (3D printing): A review of materials, methods, applications and challenges," *Compos. Part B Eng.*, vol. 143, no. February, pp. 172–196, 2018, doi: 10.1016/j.compositesb.2018.02.012.

[2]. R. Kudelski, J. Cieslik, M. Kulpa, P. Dudek, K. Zagorski, and R. Rumin, "Comparison of cost, material and time usage in FDM and SLS 3D printing methods," *2017 13th Int. Conf. Perspect. Technol. Methods MEMS Des. MEMSTECH 2017 - Proc.*, pp. 12–14, 2017, doi: 10.1109/MEMSTECH.2017.7937521.

[3]. I. Anderson, "Mechanical Properties of Specimens 3D Printed with Virgin and Recycled Polylactic Acid," *3D Print. Addit. Manuf.*, vol. 4, no. 2, pp. 110–115, 2017, doi: 10.1089/3dp.2016.0054.

[4]. O. Duncan *et al.*, "Review of auxetic materials for sports applications: Expanding options in comfort and protection," *Appl. Sci.*, vol. 8, no. 6, 2018, doi: 10.3390/app8060941.

[5]. T. Allen *et al.*, "Auxetic foams for sport safety applications," in *Procedia Engineering*, Jan. 2015, vol. 112, pp. 104–109, doi: 10.1016/j.proeng.2015.07.183.

[6]. A. Alderson, J. Rasburn, S. Ameer-Beg, P. G. Mullarkey, W. Perrie, and K. E. Evans, "An auxetic filter: A tuneable filter displaying enhanced size selectivity or defouling properties," *Ind. Eng. Chem. Res.*, vol. 39, no. 3, pp. 654–665, 2000, doi: 10.1021/ie990572w.

[7]. Y. Xue, P. Gao, L. Zhou, and F. Han, "An Enhanced Three-Dimensional Auxetic Lattice," 2020.

[8]. Y. Wang, W. Zhao, G. Zhou, and C. Wang, "Analysis and parametric optimization of a novel sandwich panel with double-V auxetic structure core under air blast loading," *Int. J. Mech. Sci.*, vol. 142–143, no. May, pp. 245–254, 2018, doi: 10.1016/j.ijmecsci.2018.05.001.

[9]. Y. Liu and H. Hu, "A review on auxetic structures and polymeric materials," *Sci. Res. Essays*, vol. 5, no. 10, pp. 1052–1063, 2010.

[10]. C. Yang, H. D. Vora, and Y. Chang, "Behavior of auxetic structures under compression and impact forces," *Smart Mater. Struct.*, vol. 27, no. 2, 2018, doi: 10.1088/1361-665X/aaa3cf.

[11]. S. Hou, T. Li, Z. Jia, and L. Wang, "Mechanical properties of sandwich composites with 3d-printed auxetic and non-auxetic lattice cores under low velocity impact," *Mater. Des.*, vol. 160, pp. 1305–1321, 2018, doi: 10.1016/j.matdes.2018.11.002.

[12]. S. F. Khan, H. Zakaria, Y. L. Chong, M. A. M. Saad, and K. Basaruddin, "Effect of infill on tensile and flexural strength of 3D printed PLA parts," *IOP Conf. Ser. Mater. Sci. Eng.*, vol. 429, no. 1, 2018, doi: 10.1088/1757-899X/429/1/012101.

[13]. C. Jiang and G. F. Zhao, "A Preliminary Study of 3D Printing on Rock Mechanics," *Rock Mech. Rock Eng.*, vol. 48, no. 3, pp. 1041–1050, 2015, doi: 10.1007/s00603-014-0612-y.
[14]. A. Papadopoulou, J. Laucks, and S. Tibbits, "Auxetic materials in design and architecture," *Nat. Rev. Mater.*, vol. 2, no. 12, p. 17078, 2017, doi: 10.1038/natrevmats.2017.78.
[15]. S. Farhangdoust, S. M. Aghaei, M. Amirahmadi, N. Pala, and A. Mehrabi, "Auxetic MEMS sensor," no. April 2020, p. 36, 2020, doi: 10.1117/12.2559330.
[16]. J. Li, V. Slesarenko, and S. Rudykh, "Auxetic multiphase soft composite material design through instabilities with application for acoustic metamaterials," *Soft Matter*, vol. 14, no. 30, pp. 6171–6180, 2018, doi: 10.1039/c8sm00874d.
[17]. M. Rismalia, S. C. Hidajat, I. G. R. Permana, B. Hadisujoto, M. Muslimin, and F. Triawan, "Infill pattern and density effects on the tensile properties of 3D printed PLA material," *J. Phys. Conf. Ser.*, vol. 1402, no. 4, 2019, doi: 10.1088/1742-6596/1402/4/044041.
[18]. B. Taherkhani, M. B. Azizkhani, J. Kadkhodapour, A. P. Anaraki, and S. Rastgordani, "Highly sensitive, piezoresistive, silicone/carbon fiber-based auxetic sensor for low strain values," *Sensors Actuators, A Phys.*, vol. 305, p. 111939, 2020, doi: 10.1016/j.sna.2020.111939.
[19]. M. F. Ahmed, Y. Li, and C. Zeng, "Stretchable and compressible piezoresistive sensors from auxetic foam and silver nanowire," *Mater. Chem. Phys.*, vol. 229, no. April 2018, pp. 167–173, 2019, doi: 10.1016/j.matchemphys.2019.03.015.
[20]. Y. Wei, S. Chen, Y. Lin, X. Yuan, and L. Liu, "Silver nanowires coated on cotton for flexible pressure sensors," *J. Mater. Chem. C*, vol. 4, no. 5, pp. 935–943, 2016, doi: 10.1039/c5tc03419a.
[21]. Y. Jiang *et al.*, "Auxetic Mechanical Metamaterials to Enhance Sensitivity of Stretchable Strain Sensors," *Adv. Mater.*, vol. 30, no. 12, pp. 1–8, 2018, doi: 10.1002/adma.201706589.
[22]. Y. Li, S. Luo, M. C. Yang, R. Liang, and C. Zeng, "Poisson Ratio and Piezoresistive Sensing: A New Route to High-Performance 3D Flexible and Stretchable Sensors of Multimodal Sensing Capability," *Adv. Funct. Mater.*, vol. 26, no. 17, pp. 2900–2908, 2016, doi: 10.1002/adfm.201505070.